

# Technical Data of In Silico Analysis of the Interaction of Dietary Flavonoid Compounds against Spike-Glycoprotein and Proteases of SARS-CoV-2

Nurbella Sofiana Altu, Cahyo Budiman \*, Rafida Razali , Ruzaidi Azli Mohd Mokhtar   
and Khairul Azfar Kamaruzaman 

Biotechnology Research Institute, Universiti Malaysia Sabah, Kota Kinabalu 88400, Sabah, Malaysia

\* Correspondence: cahyo@ums.edu.my

**Abstract:** The spike glycoprotein (S protein), 3-chymotrypsin-like protease (3CL-Pro), and papain-like protease (PL-Pro) of severe acute respiratory syndrome coronavirus 2 (SARS-CoV-2) virus are widely targeted for the discovery of therapeutic compounds against this virus. Dietary flavonoid compounds were proposed as a candidate for safe therapy for COVID-19 patients. Nevertheless, wet lab experiments for high-throughput screening of the compounds are undoubtedly time and cost consuming. This study aims to screen dietary flavonoid compounds that bind to S protein, 3CL-Pro, and PL-Pro of SARS-CoV-2. For this purpose, protein structures of the receptor-binding domain (RBD) of S protein (6M0J), 3CL-Pro (6LU7), and PL-Pro (6W9C) were retrieved from the RCSB Protein Data Bank (PDB). Twelve dietary flavonoid compounds were selected for the studies on their binding affinity to the targeted proteins by global and local docking. The docking and molecular dynamic (MD) simulations were performed using YASARA software. Out of 12 compounds, the highest binding score was observed between hesperidin against RBD S protein (−9.98 kcal/mol), 3CL-Pro (−9.43 kcal/mol), and PL-Pro (−8.89 kcal/mol) in global docking. Interestingly, MD simulation revealed that the complex between 3CL-Pro and RBD S protein has better stability than PL-Pro. This study suggests that hesperidin might have versatile inhibitory properties against several essential proteins of SARS-CoV-2. This study, nevertheless, remains to be confirmed through in vitro and in vivo assays.

**Dataset:** See Supplementary Materials.

**Dataset License:** : CC BY

**Keywords:** SARS-CoV-2; receptor-binding domain (RBD) of S protein; 3-chymotrypsin-like protease (3CL-Pro); papain-like protease (PL-Pro); molecular docking and dynamic simulation



**Citation:** Altu, N.S.; Budiman, C.; Razali, R.; Mokhtar, R.A.M.; Kamaruzaman, K.A. Technical Data of In Silico Analysis of the Interaction of Dietary Flavonoid Compounds against Spike-Glycoprotein and Proteases of SARS-CoV-2. *Data* 2022, 7, 144. <https://doi.org/10.3390/data7110144>

Academic Editor: Pufeng Du

Received: 22 August 2022

Accepted: 4 October 2022

Published: 27 October 2022

**Publisher's Note:** MDPI stays neutral with regard to jurisdictional claims in published maps and institutional affiliations.



**Copyright:** © 2022 by the authors. Licensee MDPI, Basel, Switzerland. This article is an open access article distributed under the terms and conditions of the Creative Commons Attribution (CC BY) license (<https://creativecommons.org/licenses/by/4.0/>).

## 1. Summary

Since its first emergence in December 2019, a new strain of coronavirus, namely, severe acute respiratory syndrome coronavirus 2 (SARS-CoV-2), has infected more than 500 million people worldwide [1–3]. The rapid person-to-person transmission of this virus has caused a global pandemic (COVID-19), which is currently still threatening us [3]. The World Health Organization (WHO) has reported over 6 million mortality cases globally throughout the COVID-19 pandemic caused by this virus [4]. While vaccination for COVID-19 is widely administrated, the efficacy of the vaccines remains challenging, mainly due to the emergence of new variants. Besides, some groups of people were also not eligible for vaccination due to their health issues [5]. Accordingly, a quest for safe and efficient therapeutic drugs for COVID-19 patients remains a global concern. While the cases are declining, drug discovery remains essential for addressing any possible threat by a new strain of coronavirus. Existing SARS-CoV-2 variants, such as Alpha (B.1.1.7), Beta (B.1.351),

Gamma (P.1), Delta (B.1.617.2), and Omicron (B.1.1.529), have posed an increased risk to the global community health [6].

Several studies and clinical trials have been conducted to test the feasibility of several drugs, for example, repurposed anti-malaria drugs, such as chloroquine and hydroxy-chloroquine, and even antiviral HIV drugs, such as lopinavir and ritonavir [7–9]. However, their safety and clinical proof is still questionable [10,11]. Dietary bioactive compounds are believed to be excellent sources for discovering safe and edible drug candidates against SARS-CoV-2 [12]. Earlier, dietary bioactive compounds have proven to exert multiple health benefits and counteract metabolic alterations [13]. The compounds are structurally classified into alkaloids (nitrogen-containing substances), terpenes, and phenolic compounds [14,15]. Phenolic compounds, characterized by an aromatic ring with at least one hydroxyl group, have gained broad interest. The group was demonstrated to have a wide variety of beneficial health. The compounds are structurally sub-grouped into flavonoid and non-flavonoid compounds, which are abundant in plants [13]. Among these, flavonoid compounds are widely accepted as therapeutic agents for various diseases [16]. These compounds are characterized by a benzopyrone ring bearing a phenolic or poly-phenolic group at different positions and they are widely found in fruits, herbs, stems, cereals, nuts, vegetables, flowers, and seeds [13]. More than a million flavonoid compounds are believed to exist in nature, which is an excellent tool for discovering drug candidates. Nevertheless, only about 10,000 flavonoid compounds have been identified and isolated [17].

A regimen of flavonoid-rich plants can be recommended to supplement enough flavonoids to protect and treat SARS-CoV-2 infection. This is due to the excellent immunomodulatory and anti-inflammatory activities of the natural flavonoid compounds and their inhibition properties against various inflammatory cytokines [18]. Nevertheless, translating the flavonoid compounds into the drug for COVID-19 is challenged by the issue of fishing out the best flavonoid compounds for being developed as drug candidates. The process involving thousands of compounds to screen using a conventional wet lab approach is lengthy and time consuming. Recent advancements in silico have allowed scientists to achieve quick and effective practices in many studies, one of which is in silico for drug development. Many studies involving the computation field has achieved successful preliminary results before proceeding to the next experiment, either in vivo or in vitro. Drug discovery and development is indeed a very lengthy process, and virtual screening of potential drug candidates has been regarded as a quick and accurate protocol to accelerate the preliminary stage of a drug-design plan [19].

Among the many proteins involved in the replication of the SARS-CoV-2 virus, the spike glycoprotein (S-protein) and two proteases (3-chymotrypsin-like protease/3CL-Pro and papain-like protease/PL-Pro) of this virus are considered as viable targets for being inhibited from locking the virus replication [20,21]. This is due to the essential roles of these proteins during the replication process. The receptor-binding domain (RBD) of the S-protein gains particular interest due to its crucial role in making the first interaction with the host cells through the ACE2 receptor. Indeed, many vaccines were developed based on blocking the interaction between the S-protein of SARS-CoV-2 and the ACE2 receptor of the host cells [22]. Meanwhile, 3CL-Pro and PL-Pro are essential for processing the translated polypeptide from the viral RNA to form functional viral proteins required to create a new virus particle [23]. Interestingly, the antiviral activity of the natural flavonoid compounds was also reported to be associated with their inhibition activity against SARS-CoV-2 targets for these flavonoids, including 3CL-Pro, S-protein, and PL-Pro [24]. Accordingly, screening flavonoid compounds against these three proteins is an exciting avenue for further COVID-19 drug development.

Among many natural flavonoids, dietary flavonoids are particularly interesting to explore for developing safe COVID-19 therapeutic drugs due to their edible properties. While Malaysia is blessed with mega biodiversity that serves as local sources for dietary flavonoid compounds, exploring the compounds for combating SARS-CoV-2 remains limited. Among the many types of dietary flavonoids, hesperidin, curcumin, galangin,

rutin, kaempferol, gallic acid, ellagic acid, maslinic acid, quercetin, morin, epigallocatechin gallate (ECGC), and gallic acid gallate (GCG) are among the dietary flavonoids that are promising for inhibiting the SARS-CoV-2 protein [25–33]. These compounds are also easily obtained from local food sources in Malaysia, including turmeric, pomegranate, walnut, green tea, avocado, mango, plum, honey, orange, green vegetables, guava, jackfruit, and many others. Notably, these compounds inhibit different proteins of SARS-CoV-2. To our knowledge, none of the reports, to date, simultaneously screen for the dietary flavonoid compounds targeting the SARS-CoV-2 proteins commonly targeted by flavonoid compounds (S protein, 3CL-Pro, and PL-Pro). For example, the inhibition activity of galangin was studied against 3CL-Pro [34] but not for another SARS-CoV-2 protease or the structural proteins. The simultaneous screening of the compounds should allow us to obtain dietary flavonoid compounds that block more than one SARS-CoV-2 protein. In addition, the antiviral activities of some dietary compounds above were predicted due to the involvement of the compounds in immunomodulatory and anti-inflammatory activities. The interaction of some compounds against SARS-CoV-2 proteins has not been well studied.

This paper, therefore, gives an extensive description of data on virtual analysis (*in silico*) of plant-based compounds against SARS-CoV-2 proteins to interact with RBD S protein, 3CL-Pro, and PL-Pro (Table 1). The interaction pattern of these compounds provides insight into possible inhibition properties against the target proteins of SARS-CoV-2. The rest of the paper is arranged as follows: data description is done in Section 2, and a discussion of the materials and methods used in this research is presented in Section 3.

**Table 1.** Specifications of the table.

Subject	Biological Science
Specific Subject Area	Biotechnology and Bioinformatics
Type of Data	Table Figure
How Data Were Acquired	The basic properties of the 12 dietary compounds were collected from the references (secondary data). The binding affinities of the compounds against SARS-CoV-2 proteins were obtained through docking simulation under YASARA software. The interaction map was visualized in the 2D format using LigPlot+ software. The complex structure obtained from the docking was visualized using PyMol. The dynamic of the complex was acquired through molecular dynamic simulation using YASARA software with AMBER14 forcefield for 50 nanoseconds (ns) in a solvated environment with 298 K.
Data Format	Raw (binding affinity table) Figure Analyzed
Parameters for Data Collection	The basic properties of the 12 dietary compounds were the compound names, Pubchem IDs, molecular weights, structures, and sources. Docking simulation parameters were the binding affinity of compounds against proteins (kcal/mol) and the list of residues involved in the interaction. Molecular dynamic simulation of the complex involves the parameters of the Root-Mean Square Deviation (RMSD) of protein-ligand complex (Å); Root-Mean Square Fluctuation (RMSF) of protein-ligand complex (Å), Radius of gyration (Rg) of protein-ligand complex (Å), Number of Hydrogen Bond between solute and solvent.
Description of Data Collection	The whole data were collected using a computation approach involving two-step analyses. The first step was the molecular docking (virtual screening) of the 12 dietary flavonoid compounds of three targeted SARS-CoV-2 proteins (RBD S protein, 3CL-Pro, and PL-Pro) by using YASARA software. The simulation yielded a binding energy (kcal/mol) for each compound to the target protein, representing the energy required to separate the compound from the complex. The second step involved the complex's molecular dynamic simulation (MD simulation). The simulation was performed on the best complex of protein-compound, which yielded the dynamic of the complex in the form of Root-Mean Square Deviation (RMSD), Root-Mean Square Fluctuation (RMSF), radius of gyration (Rg) of protein-ligand complexes, and also the number of hydrogen bonds between the solute and solvent based on YASARA's definition.
Data Source Location	<i>In silico</i> screening analysis and data collection were performed at the Biotechnology Research Institute, Universiti Malaysia Sabah (UMS), Kota Kinabalu, Sabah, Malaysia.
Data Accessibility	With the article and as Supplementary Materials

## 2. Data Description

Detail of the dietary flavonoid compounds to analyze in this study is shown in Table 2. These 12 compounds were selected for some reasons. Firstly, the compounds were earlier reported to be promising dietary flavonoid compounds inhibiting SARS-CoV-2 proteins. Secondly, while some compounds were reported to interact or inhibit specific SARS-CoV-2 proteins, the compounds have never been tested simultaneously against different SARS-CoV-2 proteins. Thirdly, while some of the compounds were predicted to have anti-SARS-CoV-2 activity through their immunomodulation and anti-inflammation activities, the interaction of these compounds against SARS-CoV-2 proteins has so far never been examined. Lastly, all these compounds (or their sources) are locally available in the local market of Malaysia. This availability should be easy for further studies on the compounds for further development as drugs. As shown in Table 2, the compound sizes range from 170.12 Da (gallic acid) to 610.19 Da (rutin). Accordingly, these molecules are categorized as small molecules, defined as molecules with a size of less than 1 kDa [35]. Small molecules are more favorable for drug development due to the simple process of synthesizing and ease of entering the cell target for blocking the target proteins inside the cells [36]. To note, gallic acid has not only the smallest size but also the simplest structure, containing only a single aromatic ring. The most complex structure is observed for hesperidin, with five ring structures. The source of compounds, as shown in Table 2, indicated that the compounds primarily exist in the plant (fruit or leaves). Only one compound (galangin) originated from honey. Nevertheless, all compound sources are edible; it is, therefore, acceptable to consider the compounds to be dietary compounds.

**Table 2.** Datasets include the name of the compound, chemical structure, molecular weight (g/mol), and its derivatives.

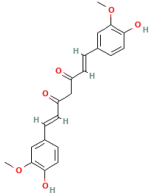
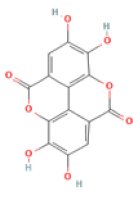
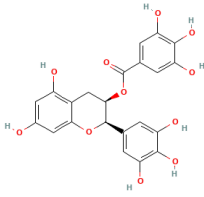
Compound	Pubchem ID	Structure	Molecular Weight (g/mol)	Sources
Curcumin	969516	 <chem>C<sub>21</sub>H<sub>20</sub>O<sub>6</sub></chem>	368.38	Turmeric ( <i>Curcuma longa</i> ) [37]
Ellagic acid	5281855	 <chem>C<sub>14</sub>H<sub>6</sub>O<sub>8</sub></chem>	302.20	Pomegranates, walnut [38]
Epigallocatechin gallate (EGCG)	65064	 <chem>C<sub>22</sub>H<sub>18</sub>O<sub>11</sub></chem>	458.37	Green tea ( <i>Camillea sinensis</i> ), nuts, avocados [39]

Table 2. Cont.

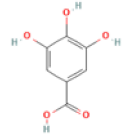
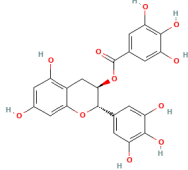
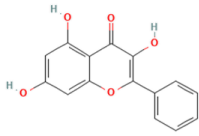
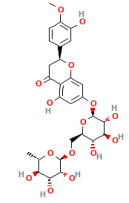
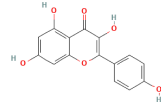
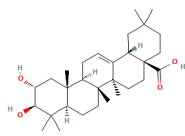
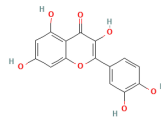
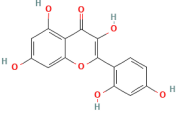
Compound	Pubchem ID	Structure	Molecular Weight (g/mol)	Sources
Gallic acid	370	 C <sub>7</sub> H <sub>6</sub> O <sub>5</sub>	170.12	Tea, mango, plum [40]
Galocatechin gallate (GCG)	5276890	 C <sub>22</sub> H <sub>18</sub> O <sub>11</sub>	458.38	Green tea ( <i>Camillea sinensis</i> ), nuts [41]
Galangin	5281616	 C <sub>15</sub> H <sub>10</sub> O <sub>5</sub>	270.24	Honey [42]
Hesperidin	10621	 C <sub>28</sub> H <sub>34</sub> O <sub>15</sub>	610.19	Orange ( <i>Citrus sinensis</i> ) [43]
Kaempferol	5280863	 C <sub>15</sub> H <sub>10</sub> O <sub>6</sub>	286.24	Green and leafy vegetables, broccoli, tea [44]
Maslinic acid	73659	 C <sub>30</sub> H <sub>48</sub> O <sub>4</sub>	472.70	Olives, edible vegetables [45]
Quercetin	5280343	 C <sub>15</sub> H <sub>10</sub> O <sub>7</sub>	302.24	Onions, tomatoes, shallots, tea [46]
Rutin	5280805	 C <sub>27</sub> H <sub>30</sub> O <sub>16</sub>	610.52	Tea, passion flower [47]

Table 2. Cont.

Compound	Pubchem ID	Structure	Molecular Weight (g/mol)	Sources
Morin	5281670	 <chem>O=C1C(=O)C(=C(O)C(O)C1OC2=CC(=C(O)C(O)C2)C3=CC(=C(O)C(O)C3)O</chem> $C_{15}H_{10}O_7$	302.23	Guava, jackfruit, tea, coffee [48]

Tables 3 and 4 show the binding energies of compounds against three SARS-CoV-2 target proteins obtained from global and local docking, respectively. Table 3 shows that the compounds interacted with the target protein with different binding energies. The lowest binding energy was found for the interaction between hesperidin and RBD S protein or 3CL-Pro or PL-Pro. The energy was calculated to be  $-9.38$  kcal/mol (RBD S protein),  $-9.43$  kcal/mol (3CL-Pro), and  $-8.89$  (PL-Pro). The lowest energy binding indicated the high stability of the complex, which implied that the compound was bound to the target protein with the highest affinity.

Table 3. Binding affinity (kcal/mol) of the plant-based compounds against three targeted proteins in global docking.

Plant-Based Compounds	Binding Affinity (kcal/mol)		
	RBD S Protein	3CL-Pro	PL-Pro
Hesperidin	$-9.38$	$-9.43$	$-8.89$
Curcumin	$-6.94$	$-6.56$	$-7.40$
Galangin	$-6.82$	$-6.88$	$-6.57$
Rutin	$-7.54$	$-8.37$	$-7.31$
Morin	$-6.83$	$-7.15$	$-6.50$
Quercetin	$-6.72$	$-7.28$	$-6.83$
Kaempferol	$-6.65$	$-7.46$	$-6.36$
Epigallocatechin gallate (EGCG)	$-7.45$	$-8.16$	$-7.21$
Gallocatechin gallate (GCG)	$-7.91$	$-8.51$	$-6.25$
Gallic acid	$-5.43$	$-5.73$	$-5.10$
Ellagic acid	$-6.78$	$-7.25$	$-6.70$
Maslinic acid	$-8.25$	$-7.69$	$-8.36$

Table 4. Binding affinity (kcal/mol) of the plant-based compounds against three targeted proteins in local docking.

Plant-Based Compounds	Binding Affinity (kcal/mol)		
	RBD S Protein	3CL-Pro	PL-Pro
Hesperidin	$-6.80$	$-8.85$	$-6.62$
Gallocatechin gallate (G.C.G.)	$-6.12$	$-4.54$	$-5.69$
Curcumin	$-6.10$	$-6.20$	$-5.00$
Ellagic acid	$-6.08$	$-6.16$	$-5.00$
Morin	$-5.86$	$-6.04$	$-5.25$
Maslinic acid	$-5.85$	$-6.10$	$-4.70$
Epigallocatechin gallate (EGCG)	$-5.62$	$-5.92$	$-5.73$
Kaempferol	$-5.55$	$-5.80$	$-4.92$
Galangin	$-5.52$	$-5.83$	$-5.00$
Rutin	$-5.52$	$-3.63$	$-5.98$
Quercetin	$-5.51$	$-6.33$	$-5.40$
Gallic acid	$-4.43$	$-4.71$	$-4.22$

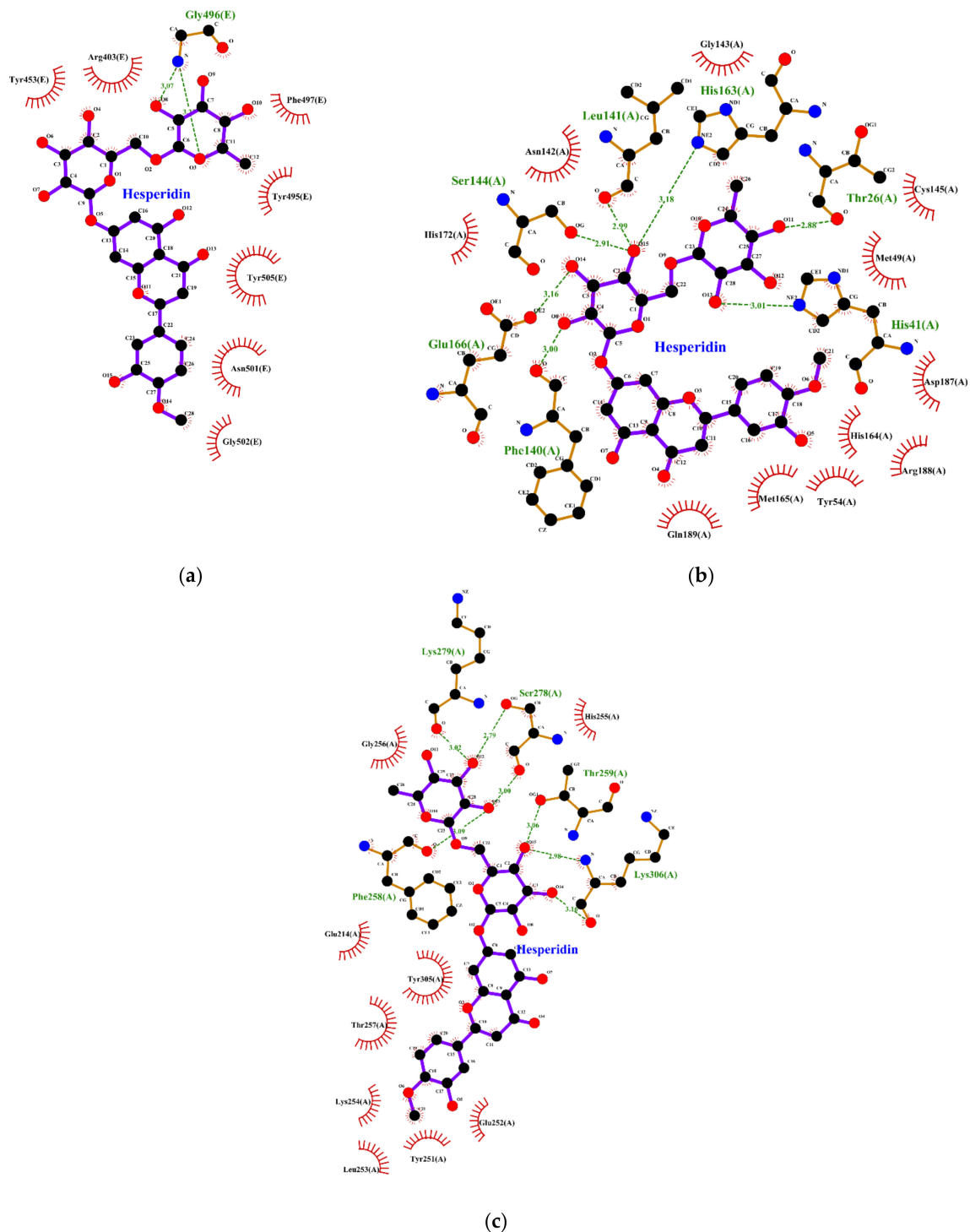
Meanwhile, gallic acid exhibited the highest binding energy for whole three proteins, with the energy of  $-5.43$  kcal/mol (RBD S protein),  $-5.73$  kcal/mol (3CL-Pro), and  $-5.10$  (PL-Pro). These energies were obtained from global docking, whereby the molecule is allowed to dock to any sites of the protein, which is energetically favorable. This approach allows us to identify possible alternative sites of the target protein to be inhibited while the predefined active sites in local docking were analyzed for insightful information.

Table 4, on the other hand, showed the binding energy of the dietary flavonoid compounds against the SARS-CoV-2 proteases obtained from the local docking approach. In the local docking, the binding sites of each target protein for the compounds to bind were identified and targeted for the docking. Interestingly, local docking also resulted in hesperidin as a compound, with the best binding energy for all the target proteins. The energy was calculated to be  $-6.80$  kcal/mol (RBD S protein),  $-8.85$  kcal/mol (3CL-Pro), and  $-6.62$  (PL-Pro). On the other hand, gallic acid exhibited the worst binding energy toward RBD S protein ( $-4.43$  kcal/mol) and PL-pro ( $-4.22$  kcal/mol). In addition, galocatechin gallate (GCG) was found to be the compound with the highest free binding energy toward 3CL-pro ( $-4.54$  kcal/mol).

Both global and local docking implied that hesperidin is a versatile compound that can dock to the RBD S protein, 3CL-Pro, and PL-Pro, with better binding energies than the other tested compounds. Nevertheless, Tables 3 and 4 show that the binding energies of hesperidin to the SARS-CoV-2 proteins resulting from global docking were slightly different from that of the local docking. As the target sites for both docking approaches were set differently during the simulation, the discrepancy in their binding energies might be related to the differences in the detailed interaction of this compound to the target protein. Figure 1 shows the 2D interaction map between hesperidin and the RBD S protein, 3CL-Pro, and PL-Pro derived from the complexes obtained from global docking.

As shown in Figure 1, the interaction between the RBD S protein and hesperidin is mainly facilitated by a hydrophobic interaction. The seven residues involved in the interaction include Arg403, Tyr453, Tyr495, Phe497, Asn501, Gly502, and Tyr505. In addition, Gly496 supports the interaction through the formation of hydrogen bonds to hesperidin, with a distance of  $3.07$  Å. This distance is in the range of appropriate distance for hydrogen bonds ( $2.7$ – $3.3$  Å) [49]. To note, Gly496, Gly502, and Tyr505 were considered critical residues for the RBD S protein to interact with the ACE2 receptor. As the map showed that hesperidin had remarkable interaction with these residues, this might be implied that hesperidin might be able to block the interaction between the RBD S protein and the receptor.

Meanwhile, the interaction between hesperidin and 3CL-Pro is contributed almost equally by both hydrophobic and non-polar interactions (Figure 1b). The eleven residues involved in the hydrophobic interaction include Met49, Tyr54, Asn142, Gly143, Cys145, His164, Met165, His172, Asp187, Arg188, and Gln189. Further, side chains of His41, Ser144, His163, and Glu166 formed hydrogen bonds to hesperidin. The distances between the interacting atoms of the residues and hesperidin were in the range of  $2.91$ – $3.18$  Å. In addition to these hydrogen bonds formed by the side chain, Thr26, Phe140, and Leu141 also formed hydrogen bonds through their main chains, ranging from  $2.88$  to  $3.00$  Å. The dyad catalytic site of 3CL-Pro (His41 and Cys145) was completely involved in the interaction. In addition, other residues involved in the interaction were in the vicinity of the dyad, which leads to an assumption that hesperidin is indeed bound around the active sites.



**Figure 1.** 2D interaction map of hesperidin against SARS-CoV-2 proteins derived from the global docking-based complex structure: (a) hesperidin and RBD S protein; (b) hesperidin and 3CL-Pro; (c) hesperidin and PL-Pro.

A similar interaction pattern was also found between PL-Pro and hesperidin, contributing almost equally by hydrophobic and hydrogen bond interactions. The hydrophobic interactions were formed by the residues of Glu214, Tyr251, Glu252, Leu253, Lys254, His255, Gly256, Thr257, and Tyr305. Meanwhile, hydrogen bonds were made by Phe258 (main chain), Thr259 (side chain), Ser278 (side and main chains), Lys279 (side chain), and Lys306 (main chain). The distance between the hydrogen bonds ranged from 2.79 to 3.16 Å. Inter-

estingly, the map showed that none of the triad catalytic sites of PL-Pro (Cys111, His272, and Asp286) were involved in the interaction. In addition, other interacting residues were also found to be located around the catalytic triad. This indicated that hesperidin binds to the substrate binding pocket of PL-Pro.

Further, the 2D interaction map between hesperidin to RBD S protein, 3CL-Pro, and PL-pro derived from the complexes obtained from local docking is shown in Figure 2. As shown in Figure 2a, the interaction between the RBD S protein and hesperidin obtained from local docking is also mainly facilitated by hydrophobic interaction. The number of residues involved in the hydrophobic interaction between the hesperidin and RBD S protein from local docking was four, namely, Ser494, Gly496, Gln498, and Tyr505, which is less than that obtained from the global docking complex. In addition, the three supporting interactions of the hydrogen bonds in the local docking-based complex were made by the OH group of Tyr449 (3.02 Å), Tyr453 (3.01 Å), and Asn501 (3.15 Å). This is different from global docking, which employed the main chain of Gly496 for the interaction. To note, while the pattern looks similar, the free binding energy obtained from the global and local docking were different (Tables 3 and 4), where the complex of global docking was energetically more stable. This might be due to the differences in the interaction pattern formed by the residues involved. To note, local docking revealed the involvement of important residues of the RBD S protein for ACE2 receptor interaction (Tyr449, Gly496, and Tyr505). Tyr449 was not involved in the interaction according to global docking. Meanwhile, the involvement of Gly496 and Tyr505 were similarly obtained from the global docking.

Interestingly, Figure 2b showed the complex of the local docking for 3CL-Pro and hesperidin yielded a slightly different interaction pattern to that derived from the global docking. Hydrophobic interactions were remarkably more dominant in the local docking-based interaction with ten residues involved (Thr25, His41, Met49, Asn142, Cys145, His164, Met165, Asp187, Arg188, and Gln189). Meanwhile, only five hydrogen bond interactions were observed between hesperidin and 3CL-Pro, which were formed by main chains of Thr24 (2.72 Å), Thr26 (3.05 and 3.10 Å), and Gly143 (3.02 Å), and the side chain of Glu166 (2.79 Å). To note, as found in global docking, the dyad catalytic sites of 3CL-Pro (Cys145 and His41) were also involved in the interaction.

Meanwhile, as shown in Figure 2c, the interaction pattern between hesperidin and PL-Pro in local-based docking is mainly due to the hydrophobic bond in Trp106, His272, Lys274, Asp286, and Leu289. Only one residue is involved in the hydrogen interaction, which is Thr265, with a distance of 3.14 Å. Interestingly, as found in the global docking complex, the local docking also revealed no interaction between hesperidin and the triad catalytic sites of PL-Pro (Cys111, His272, and Asp286). Nevertheless, the residues involved in the interaction were in the proximity of the catalytic triad.

Altogether, the list of interacting residues of RBD S protein, 3CL-Pro, and PL-Pro are listed in Table 5.

Figure 3a shows the ligand conformation obtained from both the local and global docking of hesperidin and the RBD S protein. As shown in Figure 2, the superimposition of ligands demonstrated a slightly different orientation, with an RMSD of 2.26 Å. Similarly, slight differences in the ligand conformation were also found between local and global docking of hesperidin and 3CL-Pro (Figure 3b), at 1.97 Å. Further, the superimposition of the hesperidin orientation obtained from global and local docking to PL-Pro showed a quite distinct spatial and structural orientation of the compound relative to the active site positions (Figure 3b). This might explain the differences in the residues' contribution to the interaction, as described above (Table 5). In particular, Table 5 indicates that the interacting residues of PL-Pro to hesperidin from the global and local docking are remarkably different.

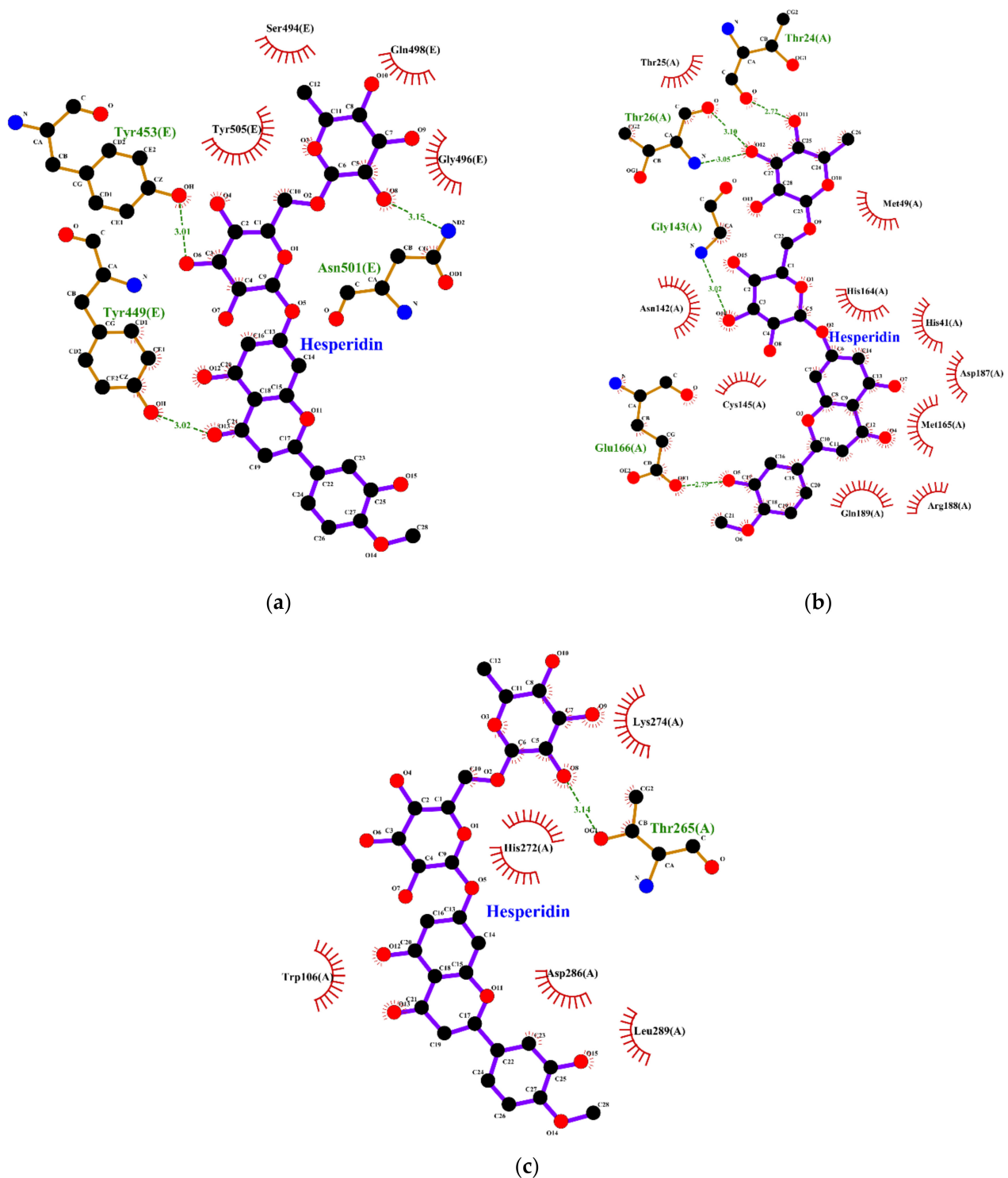


**Figure 2.** 2D interaction map of hesperidin against SARS-CoV-2 proteins derived from the local docking-based complex structure: (a) hesperidin and RBD S protein; (b) hesperidin and 3CL-Pro; (c) hesperidin and PL-Pro.

**Table 5.** The list of interacting residues of each target protein of RBD S protein, 3CL-Pro, and PL-Pro.

Target Proteins	Binding/Active Sites from References	Residues Involved in the Interaction from 2D Map	
		Global Docking	Local Docking
RBD S protein	(a) Tyr449 (b) Asn487 (c) Gly496 (d) Thr500 (e) Gly502 (f) Tyr505	a) Arg403	(a) Tyr449
		(b) Tyr453	(b) Tyr453
		(c) Tyr495	(c) Ser494
		(d) Gly496	(d) Gly496
		(e) Phe497	(e) Gln498
		(f) Asn501	(f) Asn501
3CL-Pro	(a) His41 (b) Cys145	(g) Gly502	(g) Tyr505
		(h) Tyr505	
		(a) Thr26	
		(b) His41	
		(c) Met49	(a) Thr24
		(d) Tyr54	(b) Thr25
		(e) Phe140	(c) Thr26
		(f) Leu141	(d) His41
		(g) Asn142	(e) Met49
		(h) Gly143	(f) Asn142
		(i) Ser144	(g) Cys145
		(j) Cys145	(h) Gly143
		(k) His163	(i) His164
		(l) His164	(j) Met165
		(m) Met165	(k) Glu166
		(n) Glu166	(l) Asp187
		(o) His172	(m) Arg188
		(p) Asp187	(n) Gln189
PL-Pro	(a) Cys111 (b) His272 (c) Asp286	(q) Arg188	
		(r) Gln189	
		(a) Glu214	
		(b) Tyr251	
		(c) Glu252	
		(d) Leu253	
		(e) Lys254	(a) Trp106
		(f) His255	(b) Thr265
		(g) Gly256	(c) His272
		(h) Thr257	(d) Lys274
		(i) Phe258	(e) Asp286
		(j) Thr259	(f) Leu289
		(k) Ser278	
		(l) Lys279	
(m) Tyr305			
(n) Lys306			

Further, the stability of each complex was examined under MD simulation. Figure 4 shows the Root Mean Square Deviation (RMSD) of the complexes during the simulation's 50 nanoseconds (ns). As shown in Figure 4a, the RMSD of the RBD S protein and hesperidin obtained from global docking was found to fluctuate more than that of local docking. The global docking's RMSD only began to stabilize from about 15 ns into the simulation. The average RMSD simulation time from 15 to 50 ns was  $5.44 \text{ \AA} \pm 0.77 \text{ \AA}$ .

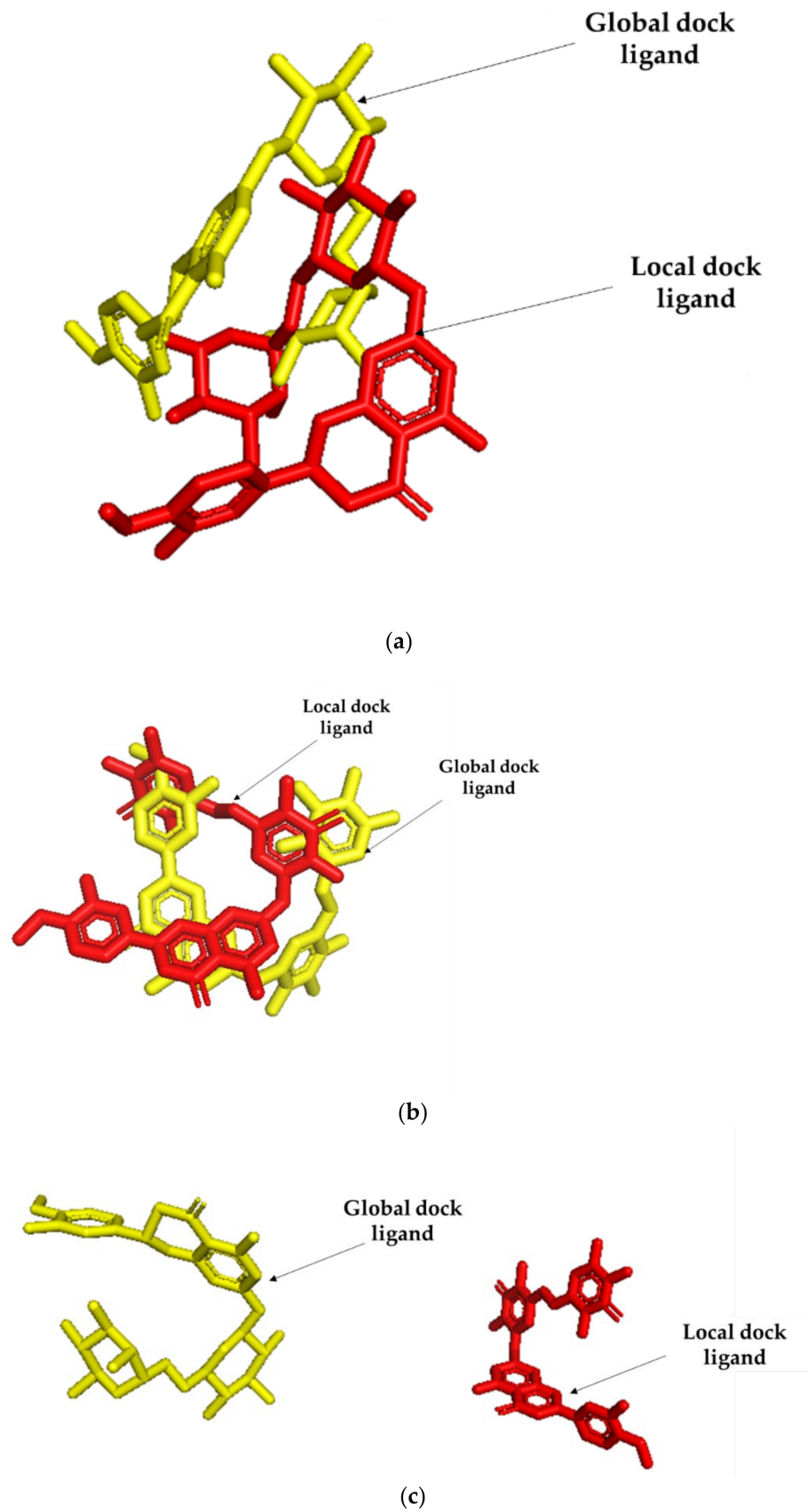


**Figure 3.** Superimposition of the hesperidin orientation obtained from the global and local docking of (a) RBD S protein; (b) 3CL-Pro; and (c) PL-Pro.

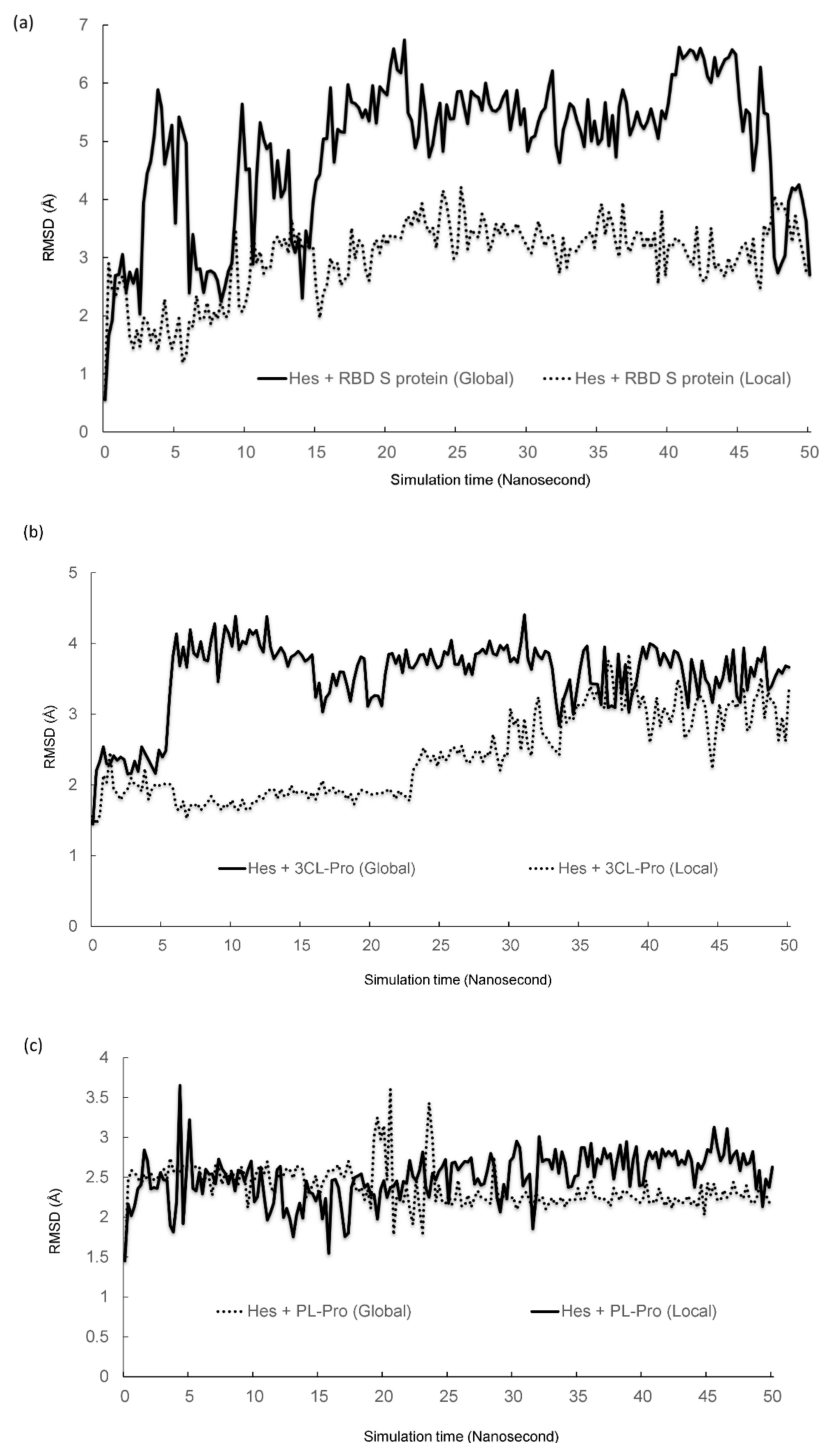


**Figure 4.** Root Mean Square Deviation (RMSD) obtained from the molecular dynamic simulation: (a) RMSD of hesperidin and RBD S protein on global and local docking; (b) RMSD of hesperidin and 3CL-Pro on global and local docking; (c) RMSD of hesperidin and PL-Pro of SARS-CoV-2 on global and local docking.

Meanwhile, the local docking-based complex of the RBD S protein and hesperidin was found to be stable starting from about 10 ns into the simulation, which was about 5 ns earlier than the global docking (Figure 4a). Overall, the average RMSD was  $3.24 \text{ \AA} \pm 0.38 \text{ \AA}$ . This indicated that even though the free binding energy of local docking was not as good as the global docking, the local docking-based complex was found to be less fluctuating, which indicates more stability during the simulation than that of the global docking complex. To

note, the fluctuation deviation was only 0.77 Å (global) and 0.38 Å (local), which is stable. According to [50], the acceptable protein fluctuation to be considered in a stable structure should be less than 3 Å. To note, the binding energy of the global docking was better than local, which were  $-9.38$  and  $-6.80$  kcal/mol, respectively (see Tables 3 and 4). While the global docking-based complex seems to fluctuate more in its RMSD than the local docking, yet remaining considerably stable, the complex is, therefore, acceptable to represent the interaction between RBD S protein and hesperidin. The detail of the RMSD changes of the RBD S protein and hesperidin obtained during simulation is available in Figure S1 and Table S1 of Supplementary Materials.

Furthermore, the RMSD values of the local and global docking-based complex of hesperidin and 3CL-Pro are shown in Figure 4b. The global docking-based complex has reached the stable RMSD from 5 ns, with an average RMSD of  $3.69 \text{ \AA} \pm 0.30 \text{ \AA}$ . Meanwhile, the RMSD range for the local docking-based complex reached stability and was less dynamic, starting from 5 ns until 23 ns into the simulation. However, more fluctuations occurred at about 23 ns, and fewer fluctuations happened at 35 ns until the end of the simulation time. Overall, the average RMSD of the complex from local docking was  $2.47 \text{ \AA} \pm 0.61 \text{ \AA}$ . As the range of RMSD fluctuation was less than 3 Å ( $0.30 \text{ \AA}$  for global and  $0.61 \text{ \AA}$  for local), this indicated that the protein was indeed stable during the 50 ns simulation.

Further, this also indicated that the complex obtained from global docking was found to be less fluctuating than the complex obtained from the local docking. To note, Tables 3 and 4 showed that the binding energy of the global docking-based complex was comparable to that of the local docking-based complex, which was  $-9.43$  and  $-8.85$  kcal/mol. Nevertheless, since the complex obtained from global docking fluctuated less, we are of the opinion that this complex is more reliable for representing the interaction between hesperidin and 3CLpro. The detail of the RMSD changes of 3CL-Pro and hesperidin obtained during simulation is available in Figure S2 and Table S2 of Supplementary Materials.

Meanwhile, the RMSD of the local and global docking-based complex for hesperidin and PL-Pro is depicted in Figure 4c. The complexes from both global and local docking reached stability from 5 ns. As shown in Figure 4c, the RMSD of the local docking-based complex was found to have an average RMSD of  $2.52 \pm 0.28 \text{ \AA}$ . Meanwhile, the global docking-based complex has an average RMSD of  $2.36 \pm 0.25 \text{ \AA}$ . Accordingly, both complexes were relatively stable during the 50 ns simulation based on the standard proposed by [50]. To note, Tables 3 and 4 show that the complex obtained from global docking has a binding energy of  $-8.89$  kcal/mol, which is relatively better than that of the complex obtained from local docking ( $-6.62$  kcal/mol). Nevertheless, since both complexes exhibited a similar RMSD fluctuation, and, consequently, a similar stability, the global docking-based complex was considered the best complex as it has a better binding energy. The detail of the RMSD changes of PL-Pro and hesperidin obtained during simulation is available in Figure S3 and Table S4 of Supplementary Materials.

Furthermore, the dynamic and stability analysis was further analyzed by looking into another critical parameter, the radius of gyration (Rg), as shown in Figure 5. The radius of gyration (Rg) is one of the important aspects to be analyzed in MD simulation as it denotes the level of compactness of the protein complex [51]. Overall, the Rg for all the complexes obtained from both global and local docking was found to be relatively stable, with only 1–2 Å deviation. In Figure 5a, the Rg value for the local docking-based complex of hesperidin and RBD S protein depicted fewer fluctuations than that of the global docking-based complex, in which it stabilized earlier compared to the global docking complex, at about 1 ns simulation. In contrast, in the global complex, fluctuations started from the 10 ns simulation time and only began to stabilize at 15 ns. The Rg value range for the local docking complex from 1 to 50 ns simulation time was between  $18.50 \text{ \AA}$  and  $18.56 \text{ \AA}$ , while the global complex ranged between  $18.66 \text{ \AA}$  and  $18.69 \text{ \AA}$ . This indicated that the local docking complex is more rigid than the global one as it showed fewer fluctuations during the 50 ns simulation run. The detail of the Rg value of the hesperidin and RBD S protein is provided in Figure S4 and Table S4 of Supplementary Materials. Further, the Rg for both

the local and global docking complexes of hesperidin and 3CL-Pro are shown in Figure 5b (the detail is provided in Figure S5 and Table S5 of Supplementary Materials). The graph shows that a smaller range in Rg values for the local docking complex, which was between 22.36 Å and 22.44 Å, compared to the global complex (22.36 Å–22.53 Å). This suggested that the local docking complex has fewer fluctuations, indicating that the complex is more stable than the global complex. Meanwhile, Figure 5c revealed that the global complex of hesperidin and PL-Pro has fewer Rg fluctuations than the local docking-based complex, in which it reached stability at about the 2 ns simulation time and showed a range of values between 23.29 Å and 23.54 Å. The Rg value range for the local complex was between 23.49 Å and 23.87 Å, which is a bit larger than that of the global complex. This suggests that the free binding energy reflects the simulation analysis, as it showed better binding than the local complex. The detail of the Rg value changes of complexes between hesperidin and PL-Pro is provided in Figure S6 and Table S6 of Supplementary Materials.

Further MD simulation analysis was done by determining the Root Mean Square Fluctuation (RMSF), as shown in Figure 6. In Figure 6a, the RMSF changes of the global and local docking-based complexes of hesperidin and RBD S protein displayed some differences (the detail is provided in Figure S7 and Table S7 of Supplementary Materials). The RMSF values of the global docking-based complex during the simulation were found to be higher as compared to the local one. Notable, some residues exhibiting remarkably high RMSF values include Tyr449 (2.43 Å), Phe486 (3.18 Å), Leu517 (3.39 Å), and His519 (3.22 Å), in which Tyr449 is an active residue of the RBD S protein for binding to ACE2 receptor. In contrast, other active sites showed low fluctuations (Asn487, Gly496, Thr500, Gly502, and Tyr505), indicating a more stable binding of the ligand to its binding pocket involving the catalytic sites. Meanwhile, the local complex showed fluctuations at the first residue of the ligand, Thr333 (3.16 Å), which indicates instability of the ligand binding to the receptor residue during the initial stage of simulation. Arg346 (2.91 Å), Asn370 (2.91 Å), Ser477 (2.86 Å), and His572 (2.72 Å) also depicted high fluctuations among the other residues of the receptor. Even though more residues were involved in giving high RMSF values for the local complex compared to the global complex, a higher range of RMSF values is shown in the global complex, thus indicating less rigidity of the binding complex. Furthermore, none of the active sites were involved in giving high peaks, which indicates that the ligand binding with the active sites is stable. In Figure 6b, both the global and local complexes of hesperidin and 3CL-Pro exhibited slightly high fluctuation at Ser1, with RMSF values of 3.15 Å and 6.38 Å, respectively (the detail is provided in Figure S8 and Table S8 of Supplementary Materials). This indicated that the ligand binding to the protein was unstable at the beginning of the simulation run. Tyr154 (3.00 Å), Arg222 (2.89 Å), and Gln306 (11.11 Å) also reflected high fluctuations for the local complex, in which the range values were still better than that of the global complex, which has several residues involving Pro52 (2.60 Å), Tyr126 (2.22 Å), Gln192 (2.16 Å), and Gln306 (12.84 Å). The RMSF values for hesperidin and PL-Pro are presented in Figure 6c with the detailed is provided in Figure S9 and Table S9 of Supplementary Materials. The amino acid residues of Arg3 (2.86 Å), Thr63 (2.15 Å), Tyr137 (2.39 Å), Lys190 (4.30 Å), Gln194 (3.00 Å), Cys224 (4.64 Å), Lys228 (5.56 Å), Gln269 (4.12 Å), and Lys315 (4.96 Å) from global protein–ligand complex exhibited more fluctuations. While in the case of local protein–ligand complex, higher RMSF peaks were presented in the Asn60 (2.53 Å), Thr63 (2.43 Å), Arg138 (2.45 Å), Lys190 (4.55 Å), Thr191 (3.76 Å), Lys228 (5.69 Å), Tyr268 (6.10 Å), and Lys315 (4.25 Å) amino acid residues. Overall, less fluctuation is depicted in the local complex compared to the global one, making it more rigid for the complex during the binding process.

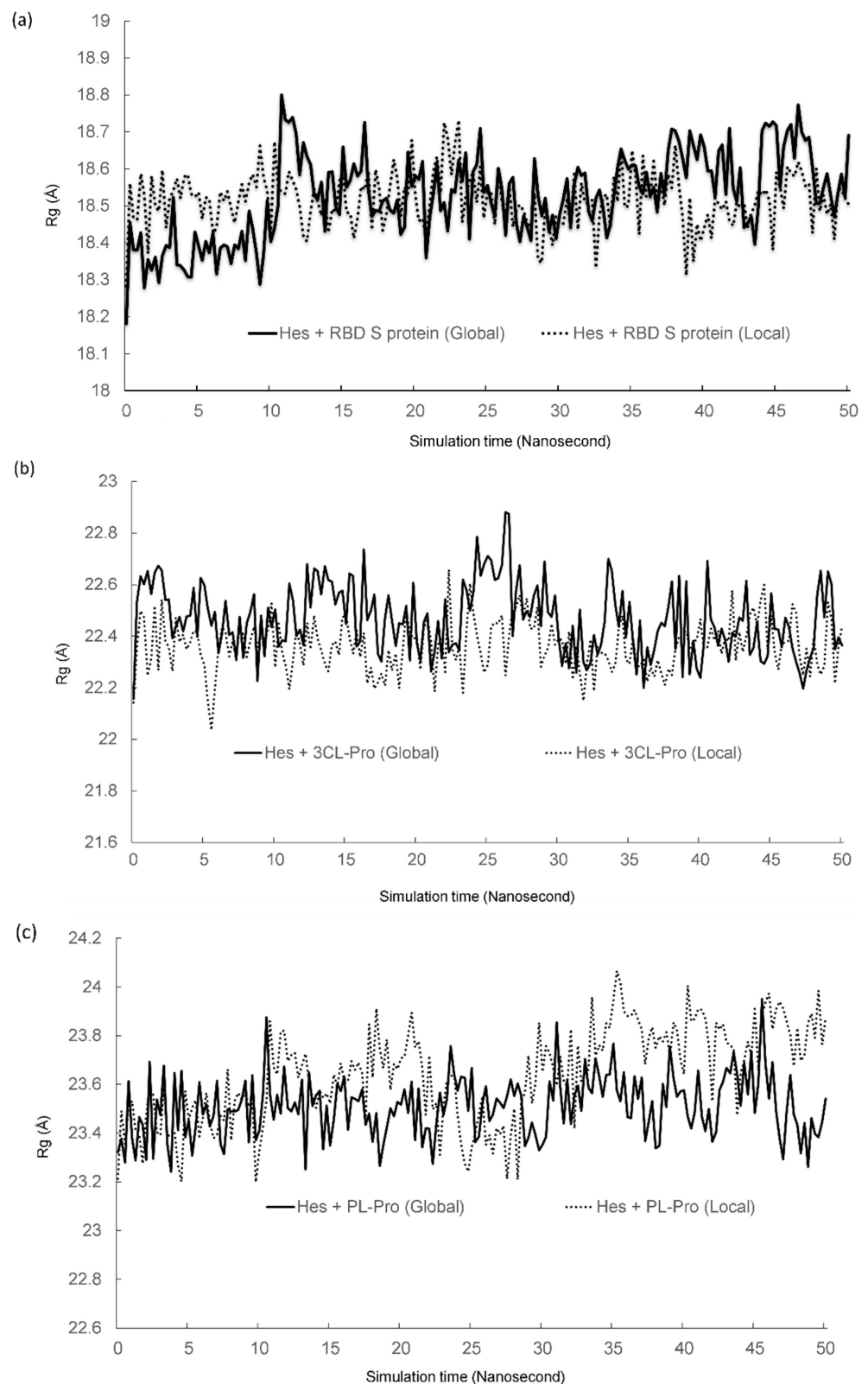


**Figure 5.** Radius of gyration (Rg) obtained from the molecular dynamic simulation: (a) radius of gyration (Rg) hesperidin and RBD S protein on global and local docking; (b) radius of gyration (Rg) of hesperidin and 3CL-Pro on global and local docking; (c) radius of gyration (Rg) of hesperidin and PL-Pro of SARS-CoV-2 on global and local docking.

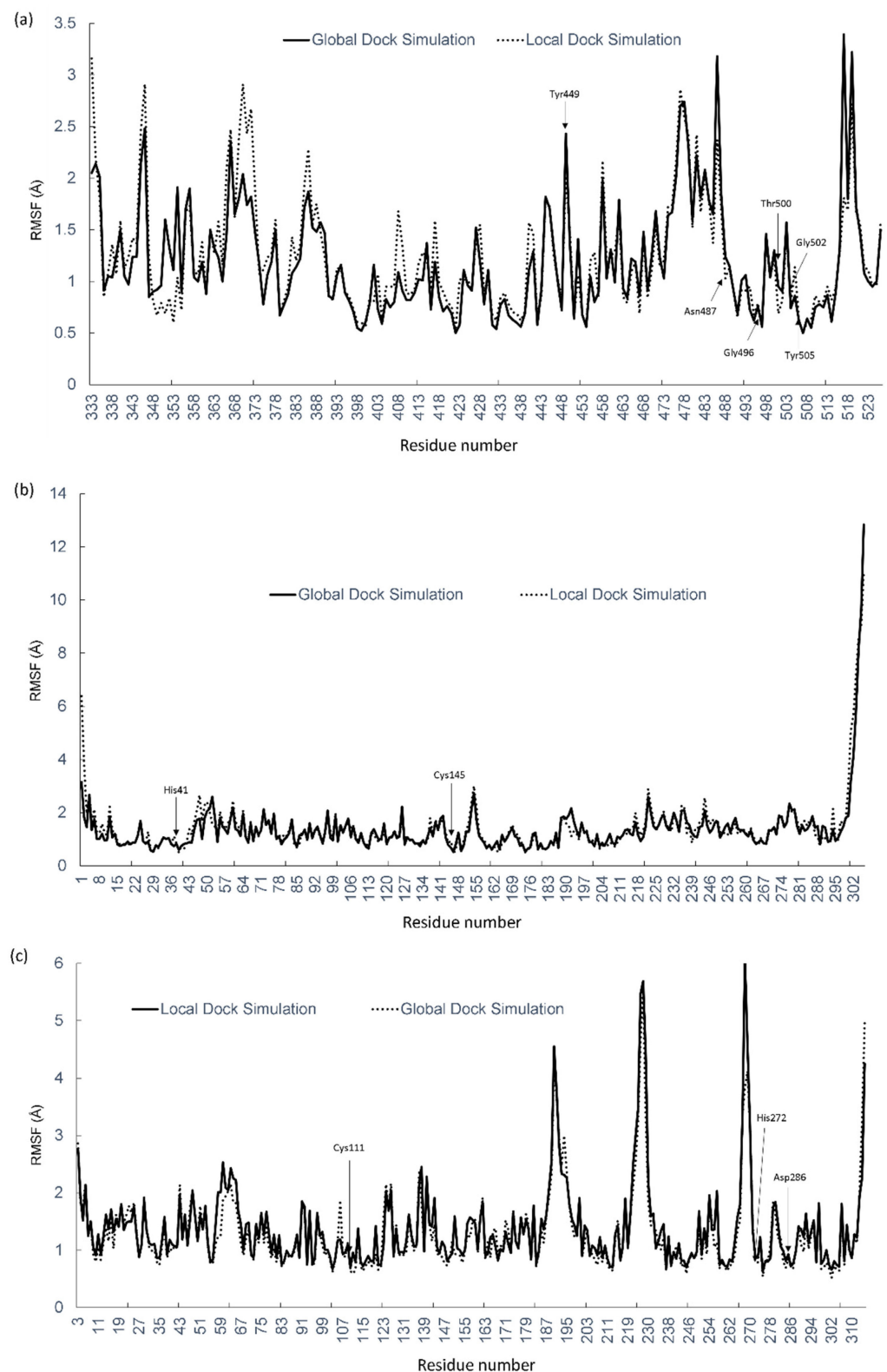


**Figure 6.** Root Mean Square Fluctuation (RMSF) obtained from the molecular dynamic simulation: (a) RMSF of hesperidin and RBD S protein on global and local docking; (b) RMSF of hesperidin and 3CL-Pro on global and local docking; (c) RMSF of hesperidin and PL-Pro of SARS-CoV-2 on global and local docking. The important residues of S-RBD for the interaction with the ACE2 receptor and the catalytic sites of 3CL-Pro and PL-Pro are labeled and indicated by the line.

RMSF values also were observed on the important residues of S-RBD for the interaction with the ACE2 receptor and the catalytic sites of 3CL-Pro and PL-Pro. The result showed that all residues exhibit RMSF values less than 3 Å during simulation (Table 6). According to [50], the acceptable protein fluctuation to be considered in a stable structure is within 1–3 Å. This indicates that the important residues or active sites of all three SARS-CoV2 proteins remain stable during the simulation. Notably, less fluctuation of the active sites in the complex implied a strong interaction with the ligand [52].

**Table 6.** The list of RMSF values involving the active site residues of each target protein in both global and local dock simulation.

Target Protein	Active Site Residues	RMSF Global (Å)	RMSF Local (Å)
RBD S protein	(a) Tyr449	2.43	2.02
	(b) Asn487	1.84	1.70
	(c) Gly496	0.76	0.79
	(d) Thr500	1.30	1.23
	(e) Gly502	0.90	0.82
	(f) Tyr505	0.86	1.14
3CL-Pro	(a) His41	0.80	0.63
	(b) Cys145	0.68	0.94
PL-Pro	(a) Cys111	0.59	0.96
	(b) His272	0.79	0.90
	(c) Asp286	0.78	0.73

To further investigate the dynamic and protein refolding, the number of hydrogen bonds between solute and solvent was analyzed (Figure 7). As shown in Figure 7, the number of hydrogen bonds during simulation for three SARS-CoV-2 proteins is relatively constant, indicating that the complexes were indeed stable. As shown in Figures 1 and 2, some hydrogen bonds also facilitate the interaction between SARS-CoV-2 proteins and the ligand. Therefore, the fluctuation in the hydrogen bond number might indicate the changes in the interaction between the protein and ligand. Unstable interaction is often characterized by the significant reduction of hydrogen bonds during simulation which consequently affects the number of hydrogen bonds [53]. Accordingly, the hydrogen bond changes during simulation are an excellent indicator to determine the complex stability. Practically, a decreasing number of hydrogen bonds in the solute, and a growing number of hydrogen bonds were presented [54]. To note, the number of hydrogen bonds depicted in Figure 7 is the total bonds in the complex, which covers the hydrogen bond between the protein and ligand and the intramolecular hydrogen bond stabilizing the structure of the protein itself. As shown in Figure 7, hydrogen bonds of all complexes of hesperidin and SARS-CoV-2 proteins (RBD S protein, 3CL-Pro or PL-Pro) were not seriously changed, which indicated that all complexes were stable during the simulation. The details of hydrogen bond changes on all complexes are provided in Figures S10–S12, as well as Tables S10–S12 of Supplementary Materials.

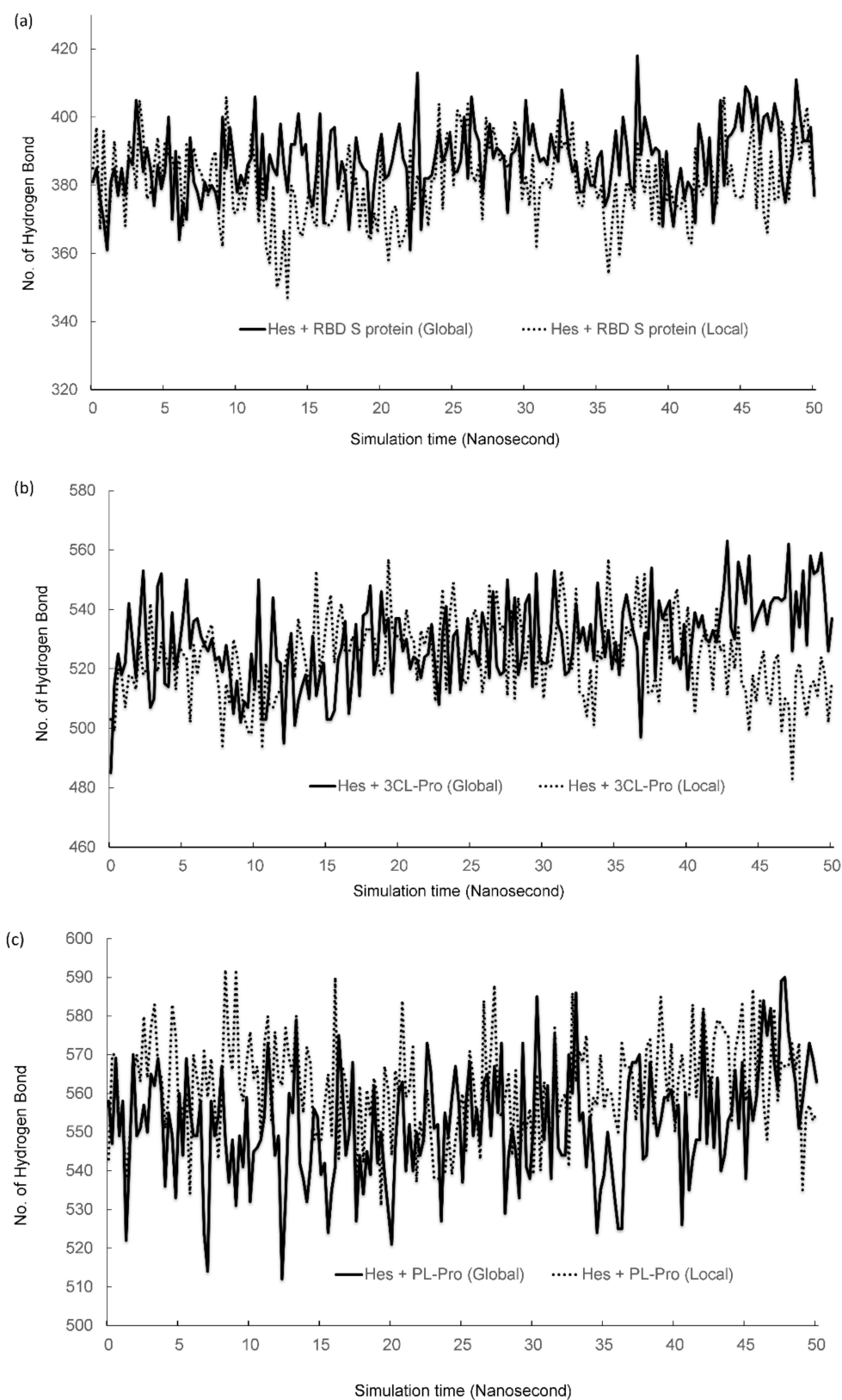


**Figure 7.** The number of hydrogen bonds between the solute and solvent obtained from the molecular dynamic simulation: (a) number of hydrogens between the solute and solvent of hesperidin and RBD S protein on global and local docking; (b) number of hydrogens between the solute and solvent of hesperidin and 3CL-Pro on global and local docking; (c) number of hydrogens between the solute and solvent of PL-Pro of SARS-CoV-2 on global and local docking.

### 3. Methods

#### 3.1. Compounds Selection

The flavonoid compounds were thoroughly selected based on a careful reading of the literature concerning the potential natural compounds against SARS-CoV-2 proteins. The structure and additional information of the compounds were retrieved from the relevant references.

#### 3.2. Protein and Ligand Preparations

Protein macromolecules of the receptor-binding domain of spike glycoprotein (RBD spike protein) and two proteases of SARS-CoV-2 that are vital in viral replication, 3-chymotrypsin-like protease (3CL-Pro) and papain-like protease (PL-Pro), were downloaded from the Research Collaboratory for Structural Bioinformatics (RCSB) protein data bank at <https://www.rcsb.org/> (accessed on 23 March 2022), with PDB IDs of 6M0J, 6LU7, and 6W9C, respectively. Water molecules were removed alongside other unnecessary molecules and atoms while ligands were prepared by using Pymol software before converting them into *yob* format in YASARA software for docking. As for the ligands, all ligand structures were downloaded in the PubChem database at [www.pubchem.ncbi.nlm.nih.gov](http://www.pubchem.ncbi.nlm.nih.gov) in 2D and 3D conformers. The format downloaded was in *sdf* format before converting them into *yob* format in YASARA software.

#### 3.3. Molecular Docking Studies

The molecular docking studies were carried out using the YASARA software package provided in the laboratory to perform virtual screening of all 12 compounds against three targeted proteins, RBD spike protein, 3CL-Pro, and PL-Pro. The docking studies were performed in two types, global and local docking, with each having different parameters and commands or scripts. Both types were conducted by using the same software. As for global docking, the simulation cell box was centered around the whole complex, and protein + ligand with 5 Å was used as in default parameter. Local docking analysis was done in which the simulation cell was centered at 90 Å, which includes only the active site residues of proteins (receptor) with sizes  $x, y, z = 18.20$  Å (RBD S protein),  $x, y, z = 15.48$  Å (3CL-Pro), and  $x, y, z = 16.61$  Å. Local docking was done to analyze the binding and interaction pattern, which only involved the active sites of the proteins and ligand and not the whole residues of the receptor. The active site residues of each protein are shown in Table 7.

**Table 7.** The active site residue information for the respective proteins involved in the study.

Protein Complex	PDB ID	Active Site Residues Literature
1. Receptor binding domain of spike glycoprotein (S RBD)	6M0J	Tyr449, Asn487, Gly496, Thr500, Gly502 & Tyr505 [55]
2. 3Chymotrypsin-like protease (3CL-Pro)	6LU7	His41 & Cys145 [56]
3. Papain-like protease (PL-Pro)	6W9C	Cys111, His272 & Asp286 [57]

#### 3.4. Molecular Dynamic Simulation (MD Simulation)

The protein–ligand complexes of hesperidin and RBD spike protein (RBD S protein), hesperidin and 3CL-Pro, and hesperidin and PL-Pro were analyzed for their dynamic stability and interaction by using the MD simulation command in the YASARA commercial package [58]. A 50 nanosecond (ns) time period was allowed for each complex, at the maximum speed, by using the *mdrunfast.mcr* command. These three complexes were chosen based on their strongest binding affinity, which was also the best ranked for each protein. AMBER14 forcefield was applied to simulate the complexes, where water molecules were

added as the solvent at a 298 K temperature. Root Mean Square Deviation (RMSD) was calculated based on the following Equation (1):

$$\text{Root Mean Square Deviation (RMSD)} = \sqrt{\frac{\sum_{i=1}^n R_i * R_i}{n}} \quad (1)$$

Root Mean Square Fluctuations (RMSF) were calculated based on the following Equation (2):

$$\text{Root Mean Square Fluctuation (RMSF)} = \sqrt{\sum_{j=1}^3 \left( \frac{1}{N} \sum_{k=1}^N P_{ikj}^2 - \bar{P}_{ij} \right)^2} \quad (2)$$

Meanwhile, the radius of gyration (Rg) was calculated based on the following Equation (3) in YASARA software:

$$\text{Radius of gyration (Rg), Mass} = \sqrt{\frac{\sum_{i=1}^N \text{Mass}_i \left( \frac{\vec{r}_i - \vec{c}}{R_i} \right)^2}{\sum_{i=1}^N \text{Mass}_i}} \quad (3)$$

The hydrogen bonds analysis based on YASARA's definition was derived by the formula below, whereby the analysis of bond energy as a function of the H-bond acceptor distance in Angstrom (Å) and another two scaling factors:

$$\text{EnergyHBo} = 25 * \frac{2.6 - \max(\text{Dis}_{H-A^{2.1}})}{0.5} * \text{Scale}_{D-H-A} * \text{Scale}_{H-A-X} \quad (4)$$

### 3.5. Data Analysis and Visualization

The results of the docking in YASARA software were provided in the output of *notepad* format and complex in *yob* format. All the ligands' docking conformation for the 11 compounds were determined by choosing the strongest binding affinity with the highest docking scores. The visualization and interaction of each complex's binding pattern were then conducted using LigPlot+ version 2.2.4 and Pymol software. The 2D output for LigPlot+ was prepared in *pdf* format and converted into *png* form.

**Supplementary Materials:** The following are available online at <https://www.mdpi.com/article/10.3390/data7110144/s1>, Figure S1: RMSD of Hes + RBD S protein on Global and Local docking, Table S1: RMSD values of Global and Local simulation between Hes + RBD S protein, Figure S2: RMSD of Hes + 3CL-Pro on Global and Local docking, Table S2: RMSD values of Global and Local simulation between Hes + 3CL-Pro, Figure S3: RMSD of Hes + PL-Pro on Global and Local docking, Table S3: RMSD values of Global and Local simulation between Hes + PL-Pro, Figure S4: Rg of Hes + RBD S protein on Global and Local docking, Table S4: Rg values of Global and Local simulation between Hes + RBD S protein, Figure S5: Rg of Hes + 3CL-Pro on Global and Local docking, Table S5: Rg values of Global and Local simulation between Hes + 3CL-Pro, Figure S6: Rg of Hes + PL-Pro on Global and Local docking, Table S6: Rg values of Global and Local simulation between Hes + PL-Pro, Figure S7: RMSF of Hes + RBD S protein on Global and Local docking, Table S7: RMSF values of Global and Local simulation between Hes + RBD S protein, Figure S8: RMSF of Hes + 3CL-Pro on Global and Local docking, Table S8: RMSF values of Global and Local simulation between Hes + 3CL-Pro, Figure S9: RMSF of Hes + PL-Pro on Global and Local docking, Table S9: RMSF values of Global and Local docking of Hes + PL-Pro, Figure S10: Number of hydrogen bond per simulation time of Hes + RBD S protein on Global and Local docking, Table S10: Number of hydrogen bond of Hes + RBD S protein, Figure S11: Number of hydrogen bond per simulation time of Hes + 3CL-Pro on Global and Local docking, Table S11: Number of hydrogen bond of Hes + 3CL-Pro, Figure S12: Number of hydrogen bond per simulation time of Hes + PL-Pro on Global and Local docking, Table S12: Number of hydrogen bond of Hes + PL-Pro.

**Author Contributions:** Writing—original draft preparation, N.S.A.; visualization, N.S.A. and R.R.; methodology, R.R.; investigation, N.S.A. and R.R.; supervision, C.B., R.A.M.M. and K.A.K.; writing—review and editing, C.B., R.A.M.M., K.A.K. and R.R.; conceptualization, C.B.; funding acquisition, C.B., R.A.M.M. and K.A.K. All authors have read and agreed to the published version of the manuscript.

**Funding:** This research was funded by Universiti Malaysia Sabah, under research grant DKC2008.

**Data Availability Statement:** The data presented in this study are available as a supplementary file.

**Acknowledgments:** We thank Herman Umbau Lindang for his technical assistance with the MD simulation.

**Conflicts of Interest:** The authors declare no conflict of interest.

## References

- Paraskevis, D.; Kostaki, E.G.; Magiorkinis, G.; Panayioti, K.G.; Sourvinos, G.; Tsiodras, S. Full-genome evolutionary analysis of the novel coronavirus (2019-nCoV) rejects the hypothesis of emergence as a result of a recent recombination event. *Infect. Genet. Evol.* **2020**, *79*, 104212. [CrossRef] [PubMed]
- Wang, Y.; Zhang, D.; Du, G.; Du, R.; Zhao, J.; Jin, Y.; Fu, S.; Gao, L.; Cheng, Z.; Lu, Q.; et al. Remdesivir in adults with severe COVID-19: A randomised, double-blind, placebo-controlled, multicentre trial. *Lancet* **2020**, *395*, 1569–1578. [CrossRef]
- Yao, X.; Ye, F.; Zhang, M.; Cui, C.; Huang, B.; Niu, P.; Liu, X.; Zhao, L.; Dong, E.; Song, C.; et al. In vitro antiviral activity and projection of optimized dosing design of hydroxychloroquine for the treatment of severe acute respiratory syndrome coronavirus 2 (SARS-CoV-2). *Clin. Infect. Dis.* **2020**, *71*, 732–739. [CrossRef] [PubMed]
- Zhang, Y.; Ma, Z.F. Impact of the COVID-19 pandemic on mental health and quality of life among local residents in Liaoning province, China: A cross-sectional study. *Int. J. Environ. Res.* **2020**, *17*, 2381. [CrossRef] [PubMed]
- Abdalla, M.; El-Arabey, A.A.; Jiang, X. What are the challenges faced by COVID-19 vaccines? *Expert Rev. Vaccines* **2021**, *21*, 5–7. [CrossRef]
- World Health Organization. Tracking SARS-CoV-2 Variants. Available online: <https://www.who.int/en/activities/tracking-SARS-CoV-2-variants/> (accessed on 17 April 2022).
- Coronavirus disease (COVID-19) pandemic (World Health Organization). Available online: <https://www.who.int/emergencies/diseases/novel-coronavirus-2019> (accessed on 17 April 2021).
- Colson, P.; Rolain, J.M.; Raoult, D. Chloroquine for the 2019 novel coronavirus SARS-CoV-2. *Int. J. Antimicrob. Agents* **2020**, *55*, 105923. [CrossRef]
- Razali, R.; Subbiah, V.J.; Budiman, C. Technical data of heterologous expression and purification of SARS-CoV-2 proteases using *Escherichia coli* system. *Data* **2021**, *6*, 99. [CrossRef]
- Magagnoli, J.; Narendran, S.; Pereira, F.; Cummings, T.H.; Hardin, J.W.; Sutton, S.S.; Ambati, J. Outcomes of hydroxychloroquine usage in United States veterans hospitalized with COVID-19. *Med* **2020**, *1*, 114–127.e3. [CrossRef]
- Mehra, M.R.; Desai, S.S.; Kuy, S.; Henry, T.D.; Patel, A.N. Cardiovascular disease, drug therapy, and mortality in COVID-19. *N. Engl. J. Med.* **2020**, *382*, 102. [CrossRef]
- Losso, J.N. The potential of dietary bioactive compounds against SARS-CoV-2 and COVID-19 induced endothelial dysfunction. *Molecules* **2020**, *27*, 1623. [CrossRef]
- Vásquez-Reyes, S.; Velázquez-Villegas, L.A.; Vargas-Castillo, A.; Noriega, L.G.; Torres, N.; Tovar, A.R. Dietary bioactive compounds as modulators of mitochondrial function. *J. Nutr. Biochem.* **2021**, *96*, 108768. [CrossRef] [PubMed]
- Andrés-Lacueva, C.; Medina-Rejon, A.; Llorach, R.; Urpi-Sarda, M.; Khan, N.; Chiva-Blanch, G.; Zamora-Ros, R.; Rotches-Ribalta, M.; Lamuela-Raventós, R.M. Phenolic Compounds: Chemistry and Occurrence in Fruits and Vegetables. In *Fruit and Vegetable Phytochemicals: Chemistry, Nutritional Value, and Stability*; Blackwell Publishing: Hoboken, NJ, USA, 2009; pp. 53–88.
- Salim, A.A.; Chin, Y.W.; Kinghorn, A.D. Drug Discovery from Plants. In *Bioactive Molecules and Medicinal Plants*; Ramawat, K.G., Merillon, J.M., Eds.; Springer: Berlin/Heidelberg, Germany, 2008; pp. 1–24.
- Razak, R.A.; Suzery, M.; Razali, R.; Amin, Z.; Mokhtar, R.A.M.; Lee, P.C.; Budiman, C. Technical data on the inhibition properties of some medicinal plant extracts towards caseinolytic protease proteolytic subunit of *Plasmodium knowlesi*. *Data Brief* **2021**, *39*, 107588. [CrossRef] [PubMed]
- Kozłowska, A.; Szostak-Wegierek, D. Flavonoids—Food sources and health benefits. *Rocz. Panstw. Zakł. Hig.* **2014**, *65*, 79–85. [PubMed]
- Alzaabi, M.M.; Hamdy, R.; Ashmawy, N.S.; Hamoda, A.M.; Alkhayat, F.; Khademi, N.N.; Joud, S.M.A.A.; El-Keblawy, A.A.; Soliman, S.S.M. Flavonoids are promising safe therapy against COVID-19. *Phytochem. Rev.* **2021**, *21*, 291–312. [CrossRef] [PubMed]
- Xu, J.; Gao, L.; Liang, H.; Chen, S.D. In silico screening of potential anti-COVID-19 bioactive natural constituents from food sources by molecular docking. *Nutrition* **2021**, *82*, 111049. [CrossRef] [PubMed]
- Rut, W.; Groborz, K.; Zhang, L.; Sun, X.; Zmudzinski, M.; Pawlik, B.; Wang, X.; Jochmans, D.; Neyt, J.; Mlynarski, W.; et al. SARS-CoV-2 Mpro inhibitors and activity-based probes for patient-sample imaging. *Nat. Chem. Biol.* **2021**, *17*, 222–228. [CrossRef]

21. Krumm, Z.A.; Lloyd, G.M.; Francis, C.P.; Nasif, L.H.; Mitchell, D.A.; Golde, T.E.; Giasson, B.; Xia, Y. Precision therapeutic targets for COVID-19. *Viol. J.* **2021**, *18*, 66. [[CrossRef](#)]
22. Osipiuk, J.; Azizi, S.A.; Dvorkin, S.; Joachimiak, A. Structure of papain-like protease from SARS-CoV-2 and its complexes with non-covalent inhibitors. *Nat. Commun.* **2021**, *12*, 743. [[CrossRef](#)]
23. Razali, R.; Asis, H.; Budiman, C. Structure-function characteristics of SARS-CoV-2 proteases and their potential inhibitors from microbial sources. *Microorganisms* **2021**, *9*, 2481. [[CrossRef](#)]
24. Kaul, R.; Paul, P.; Kumar, S.; Büsselberg, D.; Dwivedi, V.D.; Chaari, A. Promising Antiviral Activities of Natural Flavonoids against SARS-CoV-2 Targets: Systematic Review. *Int. J. Mol. Sci.* **2021**, *22*, 11069. [[CrossRef](#)]
25. Bellavite, P.; Donzelli, A. Hesperidin and SARS-CoV-2: New Light on the Healthy Function of Citrus Fruits. *Antioxidants* **2020**, *9*, 742. [[CrossRef](#)]
26. Rattis, B.A.C.; Ramos, S.G.; Celes, M.R.N. Curcumin as a potential treatment for COVID-19. *Front. Pharmacol.* **2021**, *12*, 675287. [[CrossRef](#)]
27. Jiang, Y.; Xie, Y.Z.; Peng, C.W.; Yao, K.N.; Lin, X.Y.; Zhan, S.F.; Zhuang, H.F.; Huang, H.T.; Liu, X.H.; Huang, X.F.; et al. Modeling Kaempferol as a Potential Pharmacological Agent for COVID-19/PF Co-Occurrence Based on Bioinformatics and System Pharmacological Tools. *Front. Pharmacol.* **2022**, *13*, 865097. [[CrossRef](#)]
28. Kiokias, S.; Oreopoulou, V. A Review of the Health Protective Effects of Phenolic Acids against a Range of Severe Pathologic Conditions (Including Coronavirus-Based Infections). *Molecules* **2021**, *26*, 5405. [[CrossRef](#)]
29. Abd El-Aziz, N.M.; Shehata, M.G.; Eldin Awad, O.M.; El-Sohaimy, S.A. Inhibition of COVID-19 RNA-Dependent R.N.A. Polymerase by Natural Bioactive Compounds: Molecular Docking Analysis. *Res. Sq.* **2020**, *10*, 21203.
30. Soltane, R.; Chrouda, A.; Mostafa, A.; Al-Karmalawy, A.A.; Chouaib, K.; Dhahri, A.; Pashameah, R.A.; Alasiri, A.; Kutkat, O.; Shehata, M.; et al. Strong Inhibitory Activity and Action Modes of Synthetic Maslinic Acid Derivative on Highly Pathogenic Coronaviruses: COVID-19 Drug Candidate. *Pathogens* **2021**, *10*, 623. [[CrossRef](#)]
31. Gupta, A.; Ahmad, R.; Siddiqui, S.; Yadav, K.; Srivastava, A.; Trivedi, A.; Ahmad, B.; Khan, M.A.; Shrivastava, A.K.; Singh, G.K. Flavonol morin targets host ACE2, IMP- $\alpha$ , PARP-1 and viral proteins of SARS-CoV-2, SARS-CoV and MERS-CoV critical for infection and survival: A computational analysis. *J. Biomol. Struct. Dyn.* **2022**, *40*, 5515–5546. [[CrossRef](#)]
32. Wang, Y.Q.; Li, Q.S.; Zheng, X.Q.; Lu, J.L.; Liang, Y.R. Antiviral Effects of Green Tea E.G.C.G. and Its Potential Application against COVID-19. *Molecules* **2021**, *26*, 3962. [[CrossRef](#)]
33. Ohishi, T.; Hishiki, T.; Baig, M.S.; Rajpoot, S.; Saqib, U.; Takasaki, T.; Hara, Y. Epigallocatechin gallate (E.G.C.G.) attenuates severe acute respiratory coronavirus disease 2 (SARS-CoV-2) infection by blocking the interaction of SARS-CoV-2 spike protein receptor-binding domain to human angiotensin-converting enzyme 2. *PLoS ONE* **2022**, *17*, e0271112. [[CrossRef](#)]
34. Aljarba, N.H.; Hasnanin, M.S.; Meferij, M.M.; Alkahtani, S. An in-silico investigation of potential natural polyphenols for the targeting of COVID main protease inhibitor. *J. King Saud Univ. Sci.* **2022**, *34*, 102214. [[CrossRef](#)]
35. Govardhanagiri, S.; Bethi, S.; Nagaraju, G.P. Breaking tolerance to pancreatic cancer unresponsiveness to chemotherapy. *Indian J. Med. Res.* **2021**, *154*, 653.
36. Ngo, H.X.; Garneau-Tsodikova, S. What are the drugs of the future? *Med. Chem. Comm.* **2018**, *9*, 757–758. [[CrossRef](#)] [[PubMed](#)]
37. Stanić, Z. Curcumin, a compound from natural sources, a true scientific challenge—A review. *Plant Foods Hum. Nutri.* **2017**, *72*, 1–12. [[CrossRef](#)] [[PubMed](#)]
38. Kang, I.; Buckner, T.; Shay, N.F.; Gu, L.; Chung, S. Improvements in metabolic health with consumption of ellagic acid and subsequent conversion into urolithins: Evidence and mechanisms. *Adv. Nutr.* **2016**, *7*, 961–972. [[CrossRef](#)] [[PubMed](#)]
39. Gonzalez-Alfonso, J.L.; Peñalver, P.; Ballesteros, A.O.; Morales, J.C.; Plou, F.J. Effect of  $\alpha$ -glucosylation on the stability, antioxidant properties, toxicity, and neuroprotective activity of (–)-epigallocatechin gallate. *Front. Nutr.* **2019**, *6*, 30. [[CrossRef](#)]
40. Daglia, M.; Lorenzo, A.; Nabavi, S.; Talas, Z.; Nabavi, S. Polyphenols: Well beyond the antioxidant capacity: Gallic acid and related compounds as neuroprotective agents: You are what you eat! *Curr. Pharm. Biotechnol.* **2014**, *15*, 362–372. [[CrossRef](#)]
41. Ko, S.; Jang, W.S.; Jeong, J.H.; Ahn, J.W.; Kim, Y.H.; Kim, S.; Chae, H.K.; Chung, S. (–)Gallocatechin gallate from green tea rescues cognitive impairment through restoring hippocampal silent synapses in post-menopausal depression. *Sci. Rep.* **2021**, *11*, 910. [[CrossRef](#)]
42. Aloud, A.A.; Chinnadurai, V.; Govindasamy, C.; Alsaif, M.A.; Al-Numair, K.S. Galangin, a dietary flavonoid, ameliorates hyperglycaemia and lipid abnormalities in rats with streptozotocin-induced hyperglycaemia. *Pharm. Biol.* **2018**, *56*, 302–308. [[CrossRef](#)]
43. Rehman, M.F.; Batool, A.I.; Qadir, R.; Aslam, M. Chapter 18: Hesperidin and naringenin. In *A Centum of Valuable Plant Bioactives*; Elsevier Academic Press: Cambridge, MA, USA, 2021; pp. 403–429.
44. Chen, A.Y.; Chen, Y.C. A review of the dietary flavonoid, kaempferol on human health and cancer chemoprevention. *Food Chem.* **2013**, *138*, 2099–2107. [[CrossRef](#)]
45. Lozano-Mena, G.; Sánchez-González, M.; Juan, M.; Planas, J. Maslinic acid, a natural phytoalexin-type triterpene from olives—A promising nutraceutical? *Molecules* **2014**, *19*, 11538–11559. [[CrossRef](#)]
46. Li, Y.; Yao, J.; Han, C.; Yang, J.; Chaudhry, M.; Wang, S.; Liu, H.; Yin, Y. Quercetin, inflammation, and immunity. *Nutrients* **2016**, *8*, 167. [[CrossRef](#)]
47. Ganeshpurkar, A.; Saluja, A.K. The pharmacological potential of rutin. *Saudi Pharm. J.* **2017**, *25*, 149–164. [[CrossRef](#)]
48. Caselli, A.; Cirri, P.; Santi, A.; Paoli, P. Morin: A promising natural drug. *Curr. Med. Chem.* **2016**, *23*, 774–791. [[CrossRef](#)]

49. Abelian, A.; Dybek, M.; Wallach, J.; Gaye, B.; Adejare, A. Chapter 6: Pharmaceutical Chemistry. In *Remington: The Science and Practice of Pharmacy*; Lippincott Williams and Wilkins: Philadelphia, PA, USA, 1999; pp. 105–128.
50. Parikesit, A.A.; Nurdiansyah, R.; Garrido, G. Natural products repurposing of the H5N1-based lead compounds for the most fit inhibitors against 3C-like protease of SARS-CoV-2. *J. Pharm. Pharmacogn. Res.* **2021**, *9*, 730–745. [[CrossRef](#)]
51. Swargiary, A.; Mahmud, S.; Abu Saleh, M. Screening of phytochemicals as potent inhibitor of 3-chymotrypsin and papain-like proteases of SARS-CoV-2: An in silico approach to combat COVID-19. *J. Biomol. Struct. Dyn.* **2020**, *40*, 2067–2081. [[CrossRef](#)]
52. Hosen, S.Z.; Rubayed, M.; Dash, R.; Junaid, M.; Mitra, S.; Alam, M.S.; Dey, R. Prospecting and Structural Insight into the Binding of Novel Plant-Derived Molecules of *Leea indica* as inhibitors of BACE1. *Curr. Pharm. Des.* **2018**, *24*, 3972–3979. [[CrossRef](#)]
53. Serdakowski, A.L.; Dordick, J.S. Enzyme activation for organic solvents made easy. *Trends Biotechnol.* **2008**, *26*, 48–54. [[CrossRef](#)]
54. Maiangwa, J.; Mohamad Ali, M.S.; Salleh, A.B.; Rahman, R.; Normi, Y.M.; Mohd, S.F.; Leow, T.C. Lid opening and conformational stability of T1 Lipase is mediated by increasing chain length polar solvents. *PeerJ* **2017**, *5*, e3341. [[CrossRef](#)]
55. Teli, D.M.; Shah, M.B.; Chhabria, M.T. In silico screening of natural compounds as potential inhibitors of SARS-CoV-2 main protease and spike RBD: Targets for COVID-19. *Front. Mol. Biosci.* **2021**, *7*, 599079. [[CrossRef](#)]
56. Kneller, D.W.; Phillips, G.; O'Neill, H.M.; Jedrzejczak, R.; Stols, L.; Langan, P.; Joachimiak, A.; Coates, L.; Kovalevsky, A. Structural plasticity of SARS-CoV-2 3CL Mpro active site cavity revealed by room temperature X-ray crystallography. *Nat. Commun.* **2020**, *11*, 3202. [[CrossRef](#)]
57. Báez-Santos, Y.M.; St John, S.E.; Mesecar, A.D. The SARS-coronavirus papain-like protease: Structure, function and inhibition by designed antiviral compounds. *Antiviral Res.* **2015**, *115*, 21–38. [[CrossRef](#)] [[PubMed](#)]
58. Krieger, E.; Koraimann, G.; Vriend, G. Increasing the precision of comparative models with YASARA NOVA—A self-parameterizing force field. *Proteins* **2002**, *47*, 393–402. [[CrossRef](#)] [[PubMed](#)]